Biogeosciences, 8, 55–68, 2011
www.biogeosciences.net/8/55/2011/
doi:10.5194/bg-8-55-2011

Biogeosciences

Imprint of past and present environmental conditions on microbiology and biogeochemistry of coastal Quaternary sediments

M. Beck[1], T. Riedel[1], J. Graue[1], J. Köster[1], N. Kowalski[2], C. S. Wu[3], G. Wegener[3], Y. Lipsewers[1], H. Freund[1], M. E. Böttcher[2], H.-J. Brumsack[1], H. Cypionka[1], J. Rullkötter[1], and B. Engelen[1]

[1]Institute for Chemistry and Biology of the Marine Environment (ICBM), Carl von Ossietzky University of Oldenburg, Carl-von-Ossietzky-Str. 9–11, 26129 Oldenburg, Germany
[2]Leibniz Institute for Baltic Sea Research (IOW), Geochemistry & Stable Isotope Geochemistry Group, Marine Geology Section, Seestraße 15, 18119 Warnemünde, Germany
[3]Max Planck Institute for Marine Microbiology, Celsiusstraße 1, 28359 Bremen, Germany

Received: 24 June 2010 – Published in Biogeosciences Discuss.: 15 July 2010
Revised: 17 November 2010 – Accepted: 19 December 2010 – Published: 7 January 2011

Abstract. To date, North Sea tidal-flat sediments have been intensively studied down to a depth of 5 m below seafloor (mbsf). However, little is known about the biogeochemistry, microbial abundance, and activity of sulfate reducers as well as methanogens in deeper layers. In this study, two 20 m-long cores were retrieved from the tidal-flat area of Spiekeroog Island, NW Germany. The drill sites were selected with a close distance of 900 m allowing to compare two depositional settings: first, a paleo-channel filled with Holocene sediments and second, a mainly Pleistocene sedimentary succession. Analyzing these cores, we wanted to test to which degree the paleo-environmental imprint is superimposed by present processes.

In general, the numbers of bacterial 16S rRNA genes are one to two orders of magnitude higher than those of *Archaea*. The abundances of key genes for sulfate reduction and methanogenesis (*dsr*A and *mcr*A) correspond to the sulfate and methane profiles. A co-variance of these key genes at sulfate-methane interfaces and enhanced ex situ AOM rates suggest that anaerobic oxidation of methane may occur in these layers. Microbial and biogeochemical profiles are vertically stretched relative to 5 m-deep cores from shallower sediments in the same study area, but still appear compressed compared to deep sea sediments. Our interdisciplinary analysis shows that the microbial abundances and metabolic rates are elevated in the Holocene compared to Pleistocene sediments. However, this is mainly due to present environmental conditions such as pore water flow and organic matter availability. The paleo-environmental imprint is still visible but superimposed by these processes.

Correspondence to: M. Beck
(m.beck@icbm.de)

1 Introduction

Tidal flats are coastal areas that are characterized by daily flood and ebb currents resulting in highly dynamic changes in salinity, incident light, oxygen availability and temperature. The network of sand flats, mud flats, salt marshes, islands, and tidal channels forms a transition zone between land and sea. Tidal flats are found all over the world, for example in Asia along the Korean coast, in North Africa and North America along the Atlantic coast, and in Europe in the British channel and along the North Sea coast. On a global scale, this type of landscape is of great importance due to its high primary production and organic matter remineralization rates (van Beusekom et al., 1999; Cadée and Hegeman, 2002; D'Andrea et al., 2002; de Beer et al., 2005; Loebl et al., 2007). The water column and underlying sediments are tightly coupled due to bidirectional exchange of nutrients and organic material (Huettel et al., 1998; Rusch et al., 2001; Billerbeck et al., 2006; Beck et al., 2008a).

One of the largest tidal areas of the world extends along the southern North Sea coast. It covers about 9300 km^2 and stretches more than 500 km along the coastlines of The Netherlands, Germany, and Denmark (Dittmann, 1999). The landscape of the present southern North Sea area and adjacent coastal zones developed under strong climate changes and sea level fluctuations during the Pleistocene

and Holocene. Specially the last two phases of ice advance followed by marine transgressions during warmer periods (Streif, 2004) shaped the recent landscape. The area was ice-covered during the maximum of the Saalian glaciation. During the following Eemian interglacial period the coastline was located approximately in the same area as today which is documented by shallow-marine and intertidal sediments. At the maximum of the last Weichselian glacial period the sea level fell to −130 m below its present position and the coastline was located far to the north. The main part of the southern North Sea area was not covered by ice and became part of a large, northward draining, periglacial fluvial system. The present Holocene warm period started with an initially rapid sea level rise (up to 2.1 m/100 yrs; Streif, 1990). Melting of the ice led to the drowning of the landscape with fresh water and the rising ground water table resulting in widespread peat formation. The modern coastal system was formed in the last 7500 years under the influence of a decelerating but discontinuous sea level rise interrupted by phases of stagnation or regression (Streif, 2004). Consequently, the varying past environmental conditions in this region led to a sediment record which is characterized by different depositional scenarios. For example, the alteration between a marine and freshwater environment has been influencing the biogeochemical inventory and microbial community structure.

The present biogeochemical and microbial dynamics in pore waters and sediments were studied in detail in the tidal-flat system of Spiekeroog Island within the frame of two long-term research projects (Dittmann, 1999; Rullkötter, 2009). The studies focused on surface sediments (e.g. Böttcher et al., 2000; Llobet-Brossa et al., 2002; Billerbeck et al., 2006; Al-Raei et al., 2009; Jansen et al., 2009) as well as on deeper sediment layers down to 5 m below the seafloor (mbsf) (e.g. Köpke et al., 2005; Wilms et al., 2006b; Beck et al., 2008b; Gittel et al., 2008; Røy et al., 2008). In addition, biogeochemical and microbial processes were studied in the water column and on suspended particulate matter (e.g. Liebezeit et al., 1996; Lunau et al., 2006; Dellwig et al., 2007; Rink et al., 2007; Kowalski et al., 2009; Grunwald et al., 2010). These comprehensive studies render the tidal-flat area of Spiekeroog Island into one of the presently best understood tidal-flat ecosystems worldwide.

In the Spiekeroog tidal-flat area, sulfate reduction and methanogenesis are the main terminal pathways of anaerobic organic matter remineralization in sediments down to 5 m depth. Sulfate-reducing bacteria form highly abundant and active populations in deep sandy sediments (Ishii et al., 2004; Gittel et al., 2008). Sulfate and methane show inverse depth profiles, with a methane maximum in the sulfate-depleted zone (Wilms et al., 2007; Beck et al., 2009). The population sizes of *Bacteria*, *Archaea*, sulfate reducers, and methanogens correspond well to the vertical sulfate and methane profiles (Wilms et al., 2007). The activity of sulfate reducers and methanogens and thus the turnover of organic matter are highly influenced by sedimentation rate and pore water flow (Beck et al., 2009). Profiles of the key genes for dissimilatory sulfate reduction and methanogenesis suggest ex situ anaerobic methane oxidation coupled to sulfate reduction at sulfate-methane transition zones (Wilms et al., 2007). The activity of sulfate reducers and methanogens varies in the tidal-flat area, with enhanced turnover rates at tidal-flat margins (Beck et al., 2009). Large areas in the central parts of tidal flats show low microbial activity. The highest turnover is found close to the low water line and gradually decreases across tidal-flat margins within the first tens of meters. This is due to the high availability of fresh organic matter and electron acceptors in margin sediments induced by high sedimentation rates and/or pore water flow. Overall, tidal flats and creeks were identified as a major source for methane emission (Middelburg et al., 2002).

For this study, we wanted to test to which degree the sedimentary history and thus the paleo-environment has an impact on microbial abundance, microbial activity, and pore water biogeochemistry in Quaternary sediments. The overall question was: are the past depositional conditions still reflected in present microbiological and biogeochemical processes or are they superimposed by the recent hydrology of the intertidal system? As the sediments are not isolated in space and time from the surrounding environment, hydrological and biogeochemical processes have continuously influenced the system since sediment deposition. To unravel our question, two drilling sites with different geological settings were selected which are located close to each other but differ in sediment age and paleo-environmental conditions: a paleo-channel filled with mainly Holocene sediments and a sedimentary succession with the oldest sediments deposited during the Saalian glaciation more than 130 000 years ago. A combination of geochemical and microbiological methods was used to observe the two sedimentary settings from different angles and to verify the results.

2 Material and methods

2.1 Sample collection

This study was carried out in the tidal-flat area of Spiekeroog Island, NW Germany. Based on stratigraphic information given by Sindowski (1972), two drill sites were chosen in the western tidal-flat area of Spiekeroog Island (Fig. 1). In November 2007, two 20 m long sediment cores were drilled by percussion core drilling using 1 m long polycarbonate liners (inner diameter 10 cm). Core JS-A was drilled in a deep channel incised in Pleistocene sediments and filled with Holocene material (53°43.563′ N, 7°41.249′ E). Core JS-B, taken at a distance of 900 m from JS-A, comprises sediments of the last two glacial/interglacial cycles (N 053°43.385′, E 007°42.011′).

After recovery, the core sections were immediately sealed on the drilling rig. If core sections were not completely

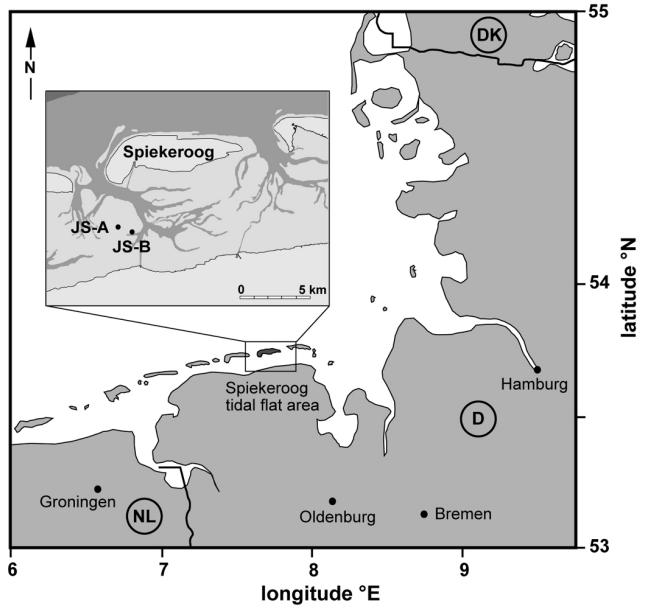

Fig. 1. Study sites JS-A and JS-B on the tidal flat Janssand located close to Spiekeroog Island in a tidal area stretching along the coasts of the Netherlands (NL), Germany (D), and Denmark (DK).

filled, a spacer was inserted into the liners to stabilize the core material. All cores were transported to a nearby laboratory where sampling was conducted within a few hours after core retrieval. Pore water for measuring chloride, sulfate, sulfide, nutrients, alkalinity, and dissolved organic carbon (DOC) was retrieved from closed core sections using Rhizon samplers (Rhizosphere research products, Wageningen, The Netherlands; Seeberg-Elverfeldt et al., 2005) which were inserted through small drill holes. Additionally, holes with a diameter of 1 cm were drilled into the liners to collect 2 cm^3 sediment samples for methane measurements. After pore water and gas sampling, cores were split lengthwise to describe the lithology and to sample sediment for further petrographical, biogeochemical and microbiological analyses. As potential contamination with seawater could not be ruled out completely for sandy sections, samples with suspicious chloride and sulfate values were disregarded.

2.2 Biogeochemical and sedimentological analyses

Pore water sulfate and chloride were measured by ion chromatography with conductivity detection (Dionex DX 300). Ammonium and silica were determined photometrically (Grasshoff et al., 1999). Total alkalinity was determined by a spectroscopic method proposed by Sarazin et al. (1999). The analytical procedures as well as precision and accuracy of the analyses are described in detail in Beck et al. (2008a).

Dissolved organic carbon (DOC) was analyzed with a multi N/C 3000 instrument (Analytik Jena AG, Jena, Germany). Pore water was 5- to 10-fold diluted with purified water, acidified with 2 N HCl and purged with synthetic air to remove inorganic carbon. For calibration, a dilution series of a DOC standard (CertiPUR®, Merck, Germany) was run parallel to the pore water samples.

For sulfide analyses, pore water aliquots were preserved in 5% Zn acetate solution after pore water extraction to prevent sulfide oxidation. Sulfide measurements were carried out by the methylene blue method (Cline, 1969) using a Specord 40 spectrophotometer (Analytik Jena AG, Jena, Germany).

For measuring methane concentrations, 2 cm^3 of sediment were transferred to gas-tight tubes filled with 20 ml sodium hydroxide solution (2.5%). Headspace samples were analyzed on a Varian CX 3400 gas chromatograph (Varian, Darmstadt, Germany) equipped with a plot-fused silica column (No. 7517; 25 m by 0.53 mm, Al_2O_3/KCl coated; Chromopack, Middleburg, The Netherlands) and a flame ionization detector.

To analyze the fractions of acid-volatile sulfur ($AVS = FeS + H_2S + HS^-$) and chromium reducible sulfur ($CRS = FeS_2 + S^0$), wet sediments were sub-sampled with cut plastic syringes and immediately fixed with Zn acetate solution (20%). A two-step distillation procedure (Fossing and Jørgensen, 1989) was applied to extract the AVS and CRS fractions separately. The composition and texture of iron sulfides was identified by electron microscopy (Quanta 400 Scanning Electron Microscope, FEI, Oregon, USA). Dried samples and an acceleration voltage of 15 kV were used for analyses.

Sedimentary structures were described by visual inspection of the cores halves. Grain size analysis was performed on fresh, ultrasonically suspended samples by means of a Fritsch Analysette 22 laser granulometer (Idar-Oberstein, Germany). Coarse material >500 µm was removed before analysis. The porosity was calculated using an empirical relationship between water content and porosity determined for a large number of samples from the same area. Water contents were determined by weighing before and after freeze drying. Total carbon and sulfur were analyzed by combustion in a CS 500 IR element analyzer (Eltra, Neuss, Germany). The total organic carbon content (TOC) was determined as the difference between total carbon and inorganic carbon measured with a CO_2 coulometer (UIC, Joliet, USA). For precision and accuracy of carbon determinations see Babu et al. (1999).

2.3 Total cell counts

Total cell counts were obtained by means of SybrGreen I as fluorescent dye according to a protocol of Lunau et al. (2005), which was adapted to sediment samples. For sample fixation, 1 cm^3 of sediment was transferred to 10 ml of a glutaraldehyde solution (1%) immediately after opening the cores. One milliliter of the homogenized sediment slurry was buffered with 2.5 µl of 50 × TAE buffer. After one or two

days of incubation, the samples were washed twice with TAE buffer. For detaching cells from particles, 300 µl methanol were added. The suspension was incubated for 15 min at 35 °C in an ultrasonic bath (Bandelin, Sonorex RK 103 H, 35 kHz, 2×320 W per period). Homogenized aliquots of 20 µl were equally dispensed on a clean microscope slide in a square of 20×20 mm. The slide was dried on a heating plate at 40 °C. A drop of 12 µl staining solution (190 µl Moviol, 5 µl SybrGreen I, 5 µl 1 M ascorbic acid in TAE buffer) was placed in the center of a 20×20 mm coverslip, which was then placed on the sediment sample. After 10 min of incubation, 20 randomly selected fields or at least 400 cells were counted for each sediment sample by epifluorescence microscopy.

2.4 DNA extraction and quantification

Total genomic DNA was extracted from 0.5 g sediment by using the FastDNA® SpinKit (Q-BIOgene, Carlsbad, Canada) according to the manufacturer's instructions. DNA concentrations were quantified fluorometrically in a microtiter plate-reader (FLUOstar Optima, BMG Labtechnologies, Offenburg, Germany) using PicoGreen (Molecular Probes, Eugene, USA). For quantification, 100 µl of PicoGreen solution (diluted 1:200 in TE buffer; pH 7.5) was added to 100 µl of DNA extract (each sample diluted 1:100 in TE buffer; pH 7.5) and subjected to a microtiter plate. Serial dilutions of Lambda-DNA (100 ng µl^{-1} to 1 ng µl^{-1}) were treated as described above and served as a calibration standard in each quantification assay. Fluorescence was measured at an excitation of 485 nm and an emission of 520 nm.

2.5 Quantitative PCR

The abundance of gene targets that are molecular markers for different phylogenetic and physiological groups of microorganisms was determined by quantitative (real-time) PCR. In detail, a modified protocol according to Wilms et al. (2007) was used to quantify the domains *Bacteria* and *Archaea*, as well as key-genes for sulfate reduction and methanogenesis, the α-units of the dissimilatory sulfite reductase (*dsr*A) and the methyl coenzyme-M reductase (*mcr*A), respectively. The latter is also used as a signature gene for anaerobic methane oxidation. All primer sequences are given in Wilms et al. (2007). Before quantification, serial dilutions of standard DNA had to be prepared for calibration. *Desulfovibrio vulgaris*^{T} (DSM 644) was chosen as the standard organism for the bacterial 16S rRNA gene and the *dsr*A gene. A culture of *Methanosarcina barkeri*^{T} (DSM 800) was used as standard for the quantification of the archaeal 16S rRNA gene and the *mcr*A gene. Genomic DNA was extracted from liquid cultures using the FastDNA® SpinKit (Q-BIOgene, Carlsbad, Canada). These DNA extracts were used to generate calibration standards for the quantification of the *dsr*A gene and the *mcr*A gene. Considering that one genome harbors only one of the key genes, the standards ranged from 4.4×10^5 to 4.4×10^0 gene copies per µl. To generate standards for quantifying *Bacteria* and *Archaea* the almost complete 16S rRNA genes were amplified prior to quantitative PCR by using the primer pairs 8f/1492r and 8f/1517r, respectively. Amplification conditions for the bacteria-specific PCR were described by Süß et al. (2004), those for the archaea-specific approach by Vetriani et al. (1999). The PCR amplicons were diluted from 1×10^8 to 1×10^0 gene copies per µl. The calibration standards were additionally amplified in every qPCR run for quantification.

Quantitative PCR amplification was performed in 25 µl volume containing 12.5 µl of the DyNAmo™ HS SYBR® Green qPCR Kit (Finnzymes Oy, Espoo, Finland), 0.2 mM of each primer, 1.5 µl PCR-water and 10 µl of the 1:100 diluted DNA templates. Thermal cycling was performed by using a Rotor-Gene, RG-3000 four channel multiplexing system (Corbett Research, Sydney, Australia) with the following parameters: 95 °C initial hold for 15 min to activate the *Taq* polymerase, followed by 50 cycles of amplification, with each cycle consisting of denaturation at 94 °C for 10 s, followed by 30 s annealing at primer-specific temperatures and the elongation step at 72 °C for 30 s. Fluorescence was measured at the end of each amplification cycle for 20 s at 82 °C. After each run, melting curves were recorded to ensure that only specific amplification had occurred.

2.6 Spiking experiments to determine the DNA recovery rate

Five sediment samples per core were selected to determine the DNA recovery rate prior to gene target quantification by qPCR (app. depth: 0.5, 4, 9, 14 and 18 mbsf). The lithologically different samples comprised intertidal sands, marine mud, fluvial clays and fluvial sands. The samples (0.5 g) and a glass-bead control were spiked with 1×10^9 cells of *Rhizobium radiobacter*. The DNA recovery rate was determined after DNA extraction and quantification of the bacterial 16S rRNA gene as described above.

2.7 Ex situ rates of anaerobic oxidation of methane (AOM) and sulfate reduction (SRR)

For rate measurements of AOM and SRR, triplicate samples of each sediment horizon were collected in glass tubes (∼8 ml), which were immediately closed with butyl rubber stoppers (Niemann et al., 2005). The samples were stored in argon-flushed Ziploc bags and kept at 8 °C. In the laboratory, ^{14}C methane (∼1 kBq) and ^{35}S sulfate (250 kBq) tracers were injected through the stopper. After incubation for 96 h, AOM incubations were stopped by transferring the samples to 50 ml glass vials filled with 25 ml sodium hydroxide (20% w/w). All glass vials were shaken thoroughly to equilibrate the pore water methane in the headspace and the sediment. After 76 h of incubation, SRR samples were

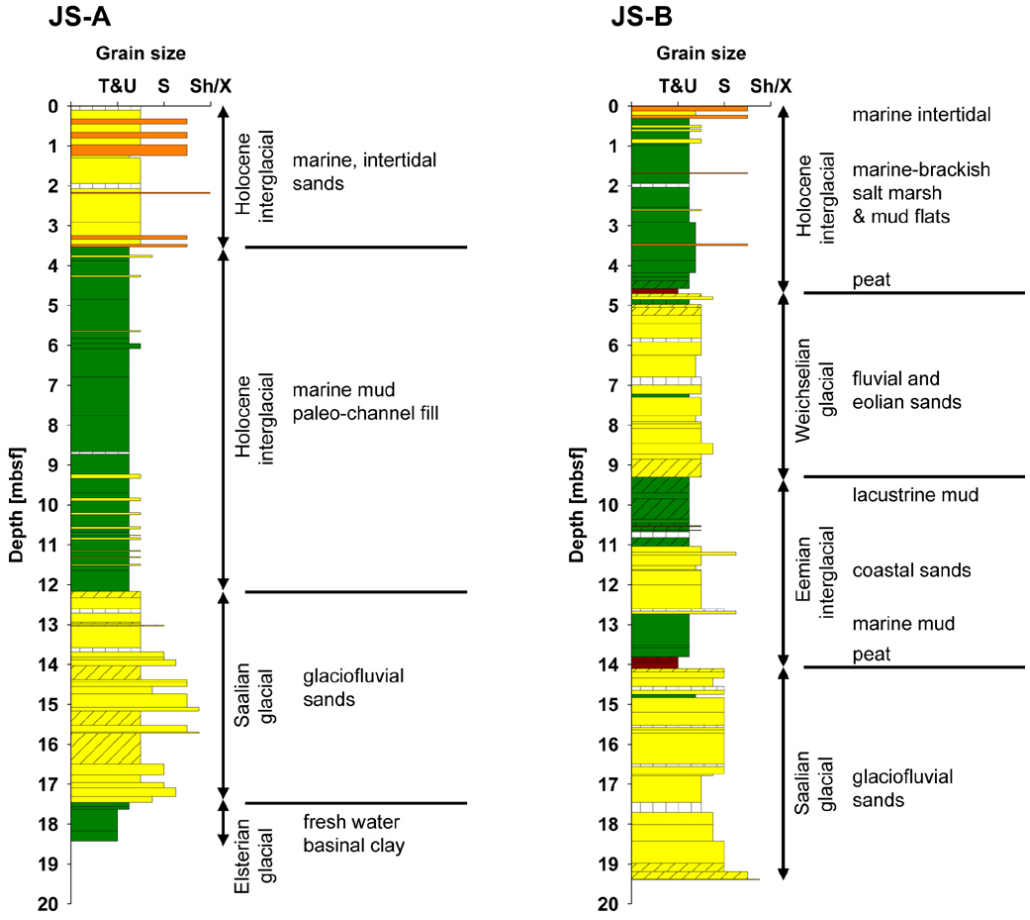

Fig. 2. Lithological profiles of the two sediment cores JS-A and JS-B. Core JS-A shows Holocene sediments filling a paleo-channel. Core JS-B displays a mainly Pleistocene sedimentary succession deposited since the Saalian glaciation more than 130 000 years ago. T&U, S, Sh indicate mud, sand, and shells, respectively. Orange: shell bed, yellow: sand, green: mud, red: peat, diagonally hatched: intervals stained by humous matter, white vertically hatched: core loss. Sediment cores were collected in November 2007.

transferred to 50 ml Falcon tubes filled with 20 ml (20% w/w) zinc acetate solution. Additionally, dead controls were prepared for AOM and SRR, in which the tracer was added to the samples directly after transferring them to their fixative. Samples were processed and rates were calculated as described by Treude et al. (2003) and Kallmeyer et al. (Kallmeyer et al., 2004). At some depths, sulfate concentration is interpolated to calculate SRR. Background thresholds for AOM and SRR were controls plus three times standard deviation and rates were only taken into account when at least two of the triplicate measurements per horizon were above detection limit.

2.8 Modeling

To obtain net sulfate reduction rates, the interstitial water gradients of dissolved sulfate were modeled for steady-state conditions using the one-dimensional modeling code PROFILE (Berg et al., 1998) as described previously (Böttcher et al., 2004). The steady-state was chosen as boundary condition, considering that the biogeochemical pore water system will adapt much faster compared to the sediment-building processes. Diffusion coefficients were corrected for in situ temperature and salinity according to Schulz (2006) and Boudreau (1997).

3 Results

3.1 Sediment structure and paleo-environment

The uppermost part of the Holocene core JS-A (Fig. 2a) consists of fine-grained, well-sorted intertidal sand with low contents of mud (i.e. <20% in the grain size fraction <63 µm) and occasional mollusk shells. The porosity is approximately 35%. The organic carbon content is generally low (<0.2%), but reaches up to 0.9% TOC in a few thin brownish layers.

The channel fill sediments between 3.5 and 12.2 mbsf consist of grey mud containing >85% silt with little fine sand. Thin, distinct layers of very fine sand occur in the lower part

of this section, but are rare in the upper part. Both top and bottom of this interval are erosive. The organic carbon content ranges from 1 to 2.4%. Due to the fine grain size, the porosity is high (avg. 56%) and permeability is low.

The underlying Pleistocene fluvial fine sands (12.2–18.4 mbsf) contain minor amounts of mud or coarse sand. They are poor in organic carbon (<0.2%). However, peat fragments, few thin layers of organic material and dispersed plant particles were found. The ages of these sands are not clearly constrained. According to Sindowski et al. (1972), a Saalian age (ca. 300 000–128 000 yrs) is likely for the lower part of this section, but an Eemian age (ca. 128 000–115 000 yrs) is possible for the upper part of the fluvial sediments. Drilling of JS-A was stopped at 18.4 mbsf in bluish green, strongly compacted clay and fine silt (1.6% TOC, ca. 22% porosity). This material belongs to the Lauenburg Clay, a ca. 325 000 year old basin sediment of the Elsterian glaciation.

Core JS-B (Fig. 2b) extends into the Saalian glaciation more than ca. 130 000 years ago. The core has a 30 cm thick surface layer of fine, shell- and mud-bearing intertidal sand underlain by Holocene brownish to medium grey and black mottled mud (Fig. 2). The presence of roots and thin shell and sand layers suggests deposition in an inter- to supratidal mud flat or salt marsh environment. Grain size distributions show two broad maxima in the fine silt (5–8 µm) and the very coarse silt range (30–60 µm). According to Chang et al. (2007), these distributions represent a mixture of fine, aggregated silty clay with a coarser sorted silt fraction. The mud contains about 1% TOC and has a porosity of ca. 55%. The base of the mud sediments at 4.6 mbsf is marked by a 12 cm thick layer of fen peat with a ^{14}C age of 5490 (±40) years BP.

Between 4.7 and 9.3 mbsf, core JS-B is dominated by light brown to grey silty fine sand and poorly sorted sandy silt of Wechselian age (ca. 115 000–10 700 yrs). The upper part contains organic matter and some plant remains. Between 9.3 and 14.1 mbsf, sediments of the Eemian interglacial (ca. 128 000–115 000 yrs) are present. From bottom to top, the Eemian sediments show a transgressive sequence with a solid layer of peat with large wood fragments and leaf remnants at the base. This is overlain by grey-brown, homogeneous, almost sand-free silt and clay with 1.2 to 3.3% TOC deposited under marine and low-energy conditions. The top of this silt and clay interval is eroded. The overlying regressive sequence consists of beige-colored, fine-grained, probably coastal sands with variable admixtures of silt (6–30%). Layers of medium to coarse sand occur near the bottom and top. The sands are followed by lacustrine, light to medium brown mud with thin layers or lenses of organic matter (TOC 1.6–3%) from 9.3 to 11.1 mbsf. The lacustrine and marine mud units are clearly distinguished by different organic carbon/sulfur ratios, ^{13}C content of the organic matter, the amount and texture of iron sulfides (especially pyrite) and micro-paleontological evidence (H. Freund, J. Köster, and M. E. Böttcher, unpublished data, 2009). The deepest part of the core from 14.1 mbsf to the bottom is formed by fluvial sand of the Saalian glacial period (ca. 300 000–128 000 yrs). It consists of beige- to grey-colored fine- to medium-grained sand. The fine fraction is mainly coarse silt and makes up 5–18%. Admixtures of coarse sand and charcoal particles are common.

3.2 Biogeochemistry

At both sites, pore water salinities drop with depth from seawater values of 30 in the upper layers to brackish values around 10 indicating saltwater-freshwater mixing (Fig. 3). Salinities are lowest near the boundary between Pleistocene and Holocene deposits due to the freshwater-dominated water regime at this time of sedimentation. Below, salinities increase again which implies the presence of a deep saltwater reservoir.

Similar to chloride, sulfate concentrations sharply decrease within the upper layers (Fig. 3). Nevertheless, the decrease in sulfate is not only due to saltwater-freshwater mixing, but also due to microbial sulfate reduction. Sulfate consumption is most pronounced at 5 to 11 mbsf in core JS-A, where sulfate shows a depletion of 14 mM after correcting for changes in chloride. Sulfide concentrations display pore water maxima in the zones of net sulfate reduction, e.g. within the top 6 m of core JS-A and the upper 12 m of core JS-B. However, part of the sulfide produced by sulfate reduction may have been lost to the sediment, most likely due to iron sulfide formation or interaction with organic matter in peat layers.

Reduced sulfur accumulated in the sediments as iron sulfides (Fig. 3). The pyrite contents (CRS) almost exactly mimic the lithological changes that correspond to TOC contents (Fig. 2) indicating that the very early diagenetic sulfur cycle was responsible for sulfide retention. Enhanced TOC contents in muddy sediments and peat layers provided the initial substrate for sulfate-reducing bacteria (Böttcher et al., 2000; Dellwig et al., 2002), and the fixation of produced sulfide indicates sufficient reactive iron to be available for pyrite formation in these sections. The occurrence of pyrite mostly in form of framboids (Fig. 4) indicates pyrite formation close to the sediment-water interface (Wilkin et al., 1996); with further pyrite formation that still went on after deeper burial, as shown by the development of euhedral pyrite crystals (Wang and Morse, 1996). In contrast, the minor AVS fraction (consisting of both, FeS and dissolved sulfide; Rickard and Morse, 2005) is not so strongly related to lithology, but follows the zones of enhanced microbial activity. AVS, however, did not dominate the reduced inorganic sulfur fraction within the investigated cores. From the covariation of lithology, TOC and CRS contents we can clearly identify the control of the very early sulfur cycle that is associated with available organic matter and reactive iron for the retention of sulfide: enhanced pyrite contents are observed

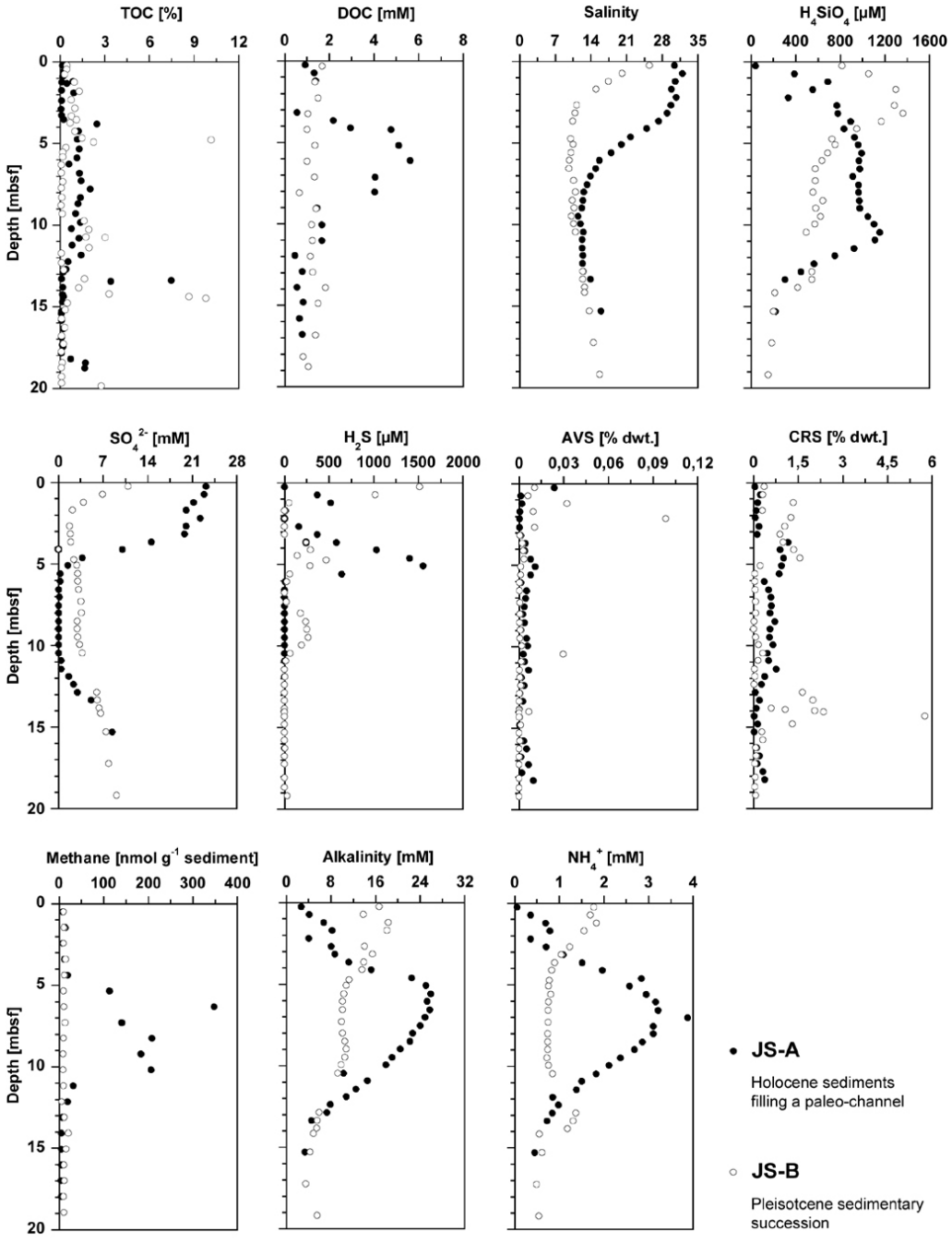

Fig. 3. Biogeochemistry at sites JS-A (filled circles) and JS-B (open circles) in the subsurface of the Janssand tidal flat: total organic carbon (TOC), dissolved organic carbon (DOC), salinity, silica, sulfate, sulfide, acid volatile sulfur (AVS), chromium reducible sulfur (CRS), methane, alkalinity, and ammonium.

in layers with high mud and TOC contents. This is in agreement with control of SRR by TOC and the sulfide retention by availability of reactive iron. We can only speculate about the fate of AVS/H_2S at the lower AOM zone at JS-A. When compared to the TOC contents and the lithology, it becomes evident, that this zone is associated with higher mud contents. Therefore, in association with enhanced pyrite contents in this part of the sediment core, we suggest, that sulfide produced by AOM may have already reacted to pyrite.

Methane concentrations are fairly low in sediment layers where sulfate is still present and are rarely exceeding 10 nmoles per gram of sediment (Fig. 3). Due to the competition for electron donors and the fact that sulfate reduction is energetically favored over methanogenesis, methanogens

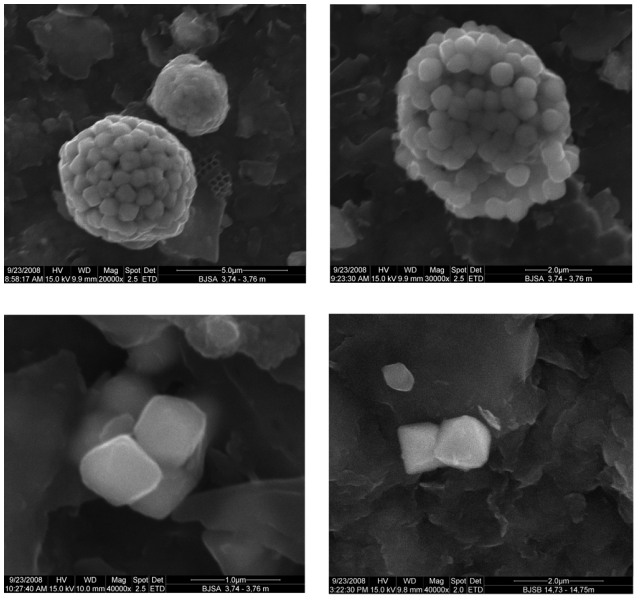

Fig. 4. Pyrite crystals from sites JS-A and JS-B. Framboidal pyrite indicates formation upon microbial sulfate reduction close to the sediment-water interface. Differences in framboid sizes are in agreement with dynamic redox conditions and oxic bottom waters (Wilkin et al., 1996). In contrast, the single euhedral crystals were formed within the sediment later upon activity of sulfate reducers (Wang and Morse, 1996).

are probably outcompeted by sulfate reducers in these layers. Only where sulfate is almost depleted, methane is found with a maximum of 350 nmol per gram of sediment (between 5 and 12 mbsf in core JS-A).

The products and indicators of organic matter remineralization such as alkalinity, DOC and ammonium show parallel trends (Fig. 3). Highest concentrations of these compounds are observed at intermediate salinities of 15 to 20 within the Holocene silt interval of core JS-A, which also hosts elevated amounts of organic matter. The DOC concentrations and the alkalinity values are therefore most likely related to the availability of degradable substrate and its degradation by sulfate reduction. The reverse covariation of alkalinity and sulfate indicates a connected process.

Dissolved silica concentrations cover a broad range from 40 to 1400 µM (Fig. 3). Highest concentrations are associated with the Holocene salt marsh sediments. Silica enrichment in marine and estuarine pore waters results from the dissolution of biogenic silica after deposition and burial of diatom frustules (Dixit and van Cappellen, 2002; Gallinari et al., 2002). Dissolved silica may therefore serve as a chemo(litho)stratigraphic marker to distinguish marine from non-marine deposits. In fact, concentrations of dissolved silica greater than 800 µM occur within Holocene deposits, while non-marine deposits have lower concentrations. However, an exact assignment of silica concentrations to discrete lithologies is hampered as boundaries are blurred by diffusional exchange.

3.3 Microbial abundance

The depth profiles of bacterial and archaeal 16S rRNA genes obtained by quantitative (real-time) PCR generally follow the total cell counts (Fig. 5). While core JS-B exhibits constant depth profiles for all quantifications, a drop by one order of magnitude was found in JS-A at 11 mbsf. This coincides with the lithological boundary between Holocene mud-rich and Pleistocene sandy sediments. In general, the bacterial 16S rRNA gene copy numbers are one to two orders of magnitude higher than those of *Archaea*. The distribution of *mcr*A genes corresponds to the numbers of archaeal 16S rRNA genes in both cores. In contrast to core JS-B, core JS-A exhibits a high proportion of *mcr*A genes in comparison to the number of archaeal 16S rRNA genes. This suggests that most of the *Archaea* in core JS-A harbor the molecular signature gene for methanogenesis or anaerobic methane oxidation while most of the *Archaea* in core JS-B are probably not capable of these processes.

A similar trend was observed for the *dsr*A gene, the molecular marker for sulfate reduction. While the numbers of *dsr*A genes are one to three orders of magnitude lower than the numbers of bacterial 16S rRNA genes in core JS-A, they are up to four orders of magnitude lower in core JS-B. This suggests that at site JS-A a higher proportion of bacteria is able to use sulfate as electron acceptor for anaerobic respiration than in core JS-B.

The abundances of the described gene targets correspond well with the sulfate and methane profiles along the depth profiles of the cores. At site JS-A, increasing numbers of bacterial 16S rRNA genes and *dsr*A genes were detected around the two sulfate-methane transition zones (Fig. 6). The distributions of *mcr*A genes and archaeal 16S rRNA genes show similar peaks with depth. The co-occurrence of both key genes for anaerobic oxidation of methane at the expense of sulfate suggests that anaerobic oxidation of methane may take place at the sulfate-methane transition zones. In core JS-B, the relationship of sulfate to the number of *dsr*A genes is reflected by their numerical increase around 4 mbsf. Further, the sulfate minimum matches the elevated sulfide concentrations (Fig. 3) suggesting the presence of an active sulfate reducing community in this layer.

In general, there is a methodological divergence of direct cell counting and molecular quantification (Fig. 5). The difference between total cell counts and molecularly determined numbers of gene copies may have several reasons. First, direct counting by using fluorescent dyes overestimates the actual numbers in most cases due to unspecific staining of sediment particles (Morono et al., 2009). Second, the primers used do not target all sequences and may discriminate certain groups of organisms. Third, DNA extraction from subsurface sediments is always characterized by a low efficiency

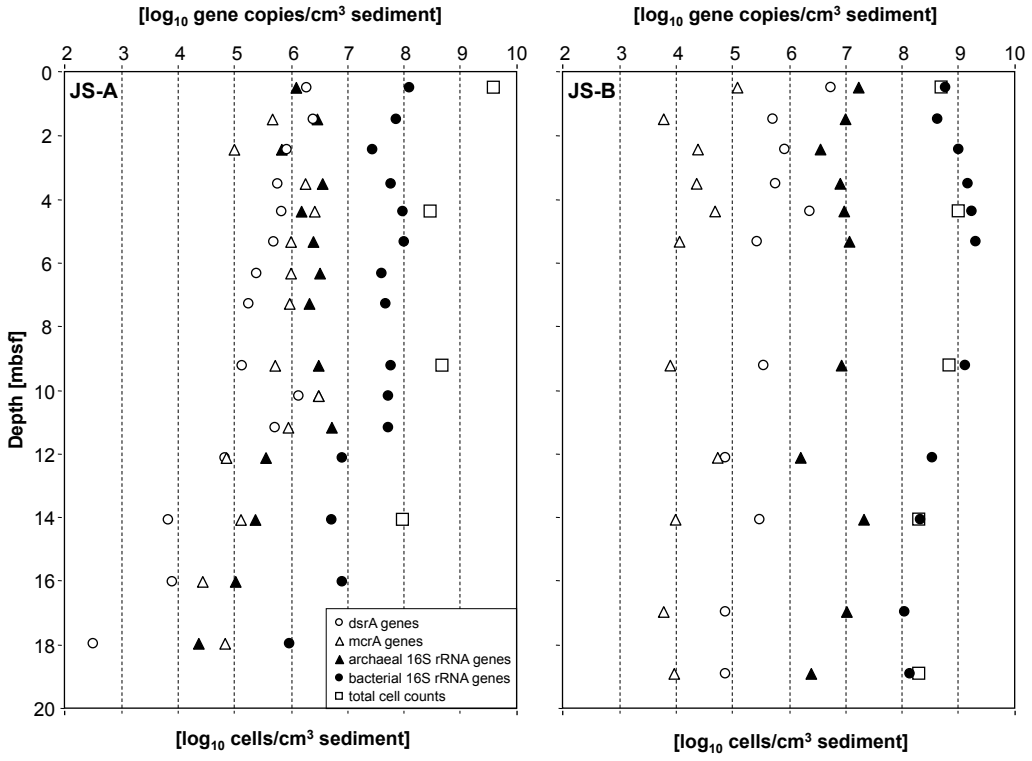

Fig. 5. Total cell counts and abundances of bacterial and archaeal 16S rRNA gene copies, *dsr*A and *mcr*A gene copies at sites JS-A and JS-B. Total cell counts were directly obtained by means of SybrGreen staining, whereas others were obtained by quantitative PCR. Core JS-B exhibits constant depth profiles for all quantifications. In contrast, a drop in all quantifications by one order of magnitude was found below the lithological boundary at 12 mbsf of core JS-A.

(D'Hondt et al., 2004). A spiking experiment with five representative samples per core and a defined number of cells indicated a recovery rate of 33–82% after DNA extraction and qPCR amplification. This rate may even be lower for indigenous microorganisms as many of them are probably attached to particles or protected by exopolymeric substances.

3.4 Microbial activity

At site JS-A, ex situ sulfate reduction rates are highest in the upper 5 mbsf where sulfate is available at almost seawater concentrations (Fig. 6). Below, sulfate reduction rates are diminished due to the lack of sulfate. However, below 12 mbsf, the reappearing sulfate is reduced at rates similar to those in the upper 5 mbsf. At site JS-B, ex situ sulfate reduction rates are highest in the Holocene sediment layers down to about 4 mbsf. Significant, but low rates were also measured at 9, 13 and 18 mbsf, whereas in the intervals between these horizons sulfate reduction rates were below the detection limit.

Modeled net sulfate reduction rates from pore water sulfate profiles are ten to hundred times lower compared to gross rates reported for highly active surface sediments in the study area (Al-Raei et al., 2009; Beck et al., 2009). Modeling the top 6 m of core JS-A and the top 2.7 m of core JS-B yields depth-integrated sulfate reduction rates of 0.1 and 0.3 mmol m^{-2} d^{-1}, respectively (considering a pelagic sulfate concentration of 26 mM). In addition, pore water modeling gave volumetric rates of 1.2 nmol cm^{-3} d^{-1} (JS-B) to 16 nmol cm^{-3} d^{-1} (JS-A), which are slightly higher than the gross rates measured with radio tracers (Fig. 6).

Ex situ anaerobic methane oxidation rates peak at about 5 mbsf and 11 mbsf at site JS-A (Fig. 6). This fits nicely with the sulfate-methane transition zones and the slightly increased numbers of *mcr*A and *dsr*A gene copies close to these interfaces. In contrast, AOM rates are very low at site JS-B. This may be due to the low methane concentration in this core where sulfate is still present at all depths.

4 Discussion

Sedimentological, biogeochemical, and microbiological investigations lead to a comprehensive picture. While the imprint of past environmental conditions on core JS-B is not as predominant as initially expected, microbial abundance and activity is elevated at sedimentological boundaries in core JS-A. Both, in turn, shape the biogeochemical depth profiles. The sulfate input from the water column to the surface sediments and the replenishment of sulfate in deep sediment

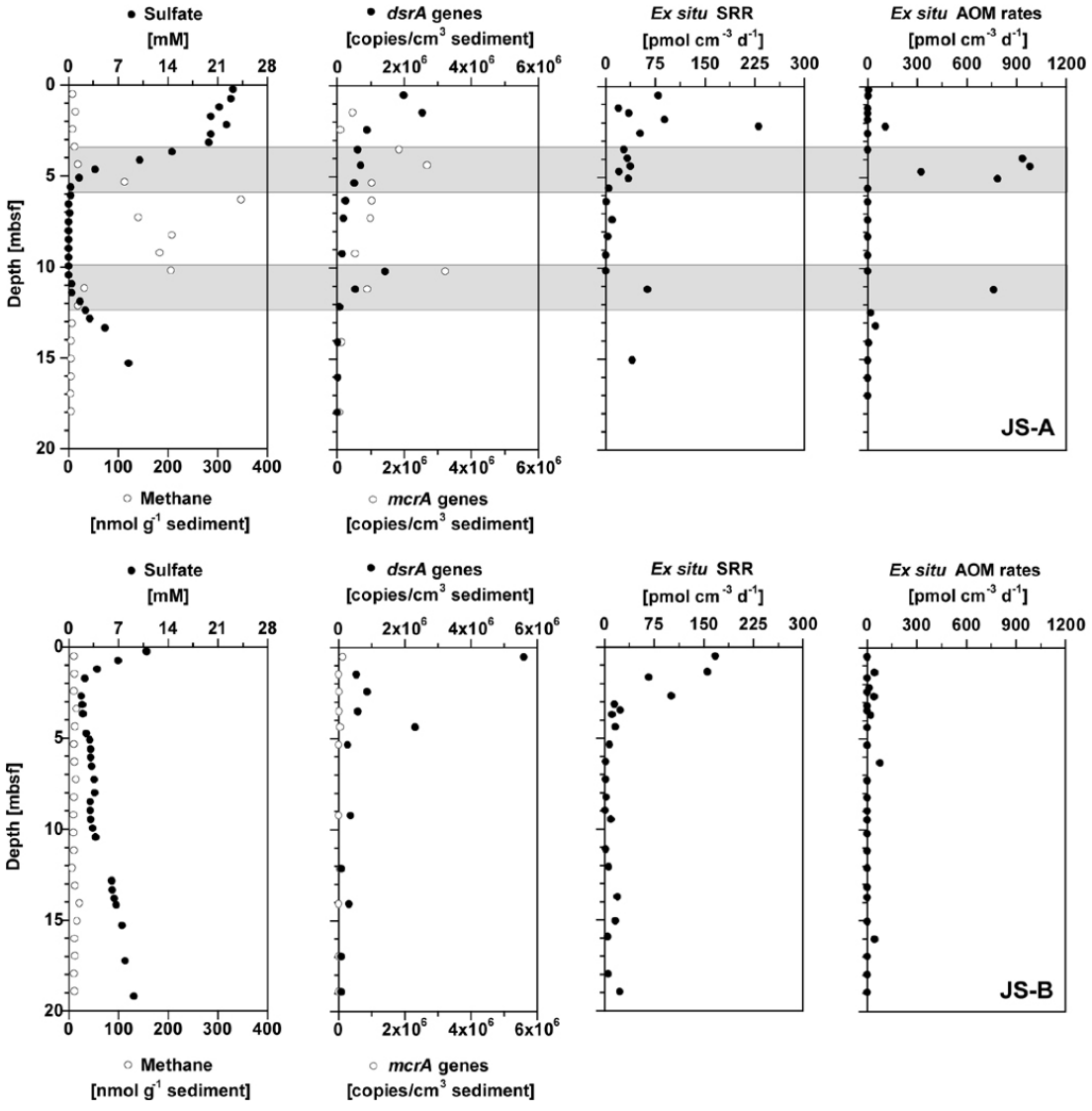

Fig. 6. Sulfate and methane concentrations, copy numbers of *dsr*A and *mcr*A genes, ex situ sulfate reduction rates (SRR), and ex situ rates of anaerobic oxidation of methane (AOM) at sites JS-A and JS-B. The grey bars highlight the sulfate-methane interfaces. The same scales are used for both sites. Enhanced ex situ SRR are coupled to higher *dsr*A copy numbers and consumption of sulfate, whereas a higher abundance of *mcr*A genes corresponds to methane concentrations. Site JS-A shows two sulfate-methane transition zones with detectable methane consumption and elevated ex situ AOM rates.

layers results in enhanced activity of sulfate reducers. In previous investigations of approximately 5 m-long sediment cores, increased numbers of *dsr*A and *mcr*A gene copies at the sulfate-methane transition zone led to the suggestion that sulfate-dependent anaerobic oxidation of methane may occur (Thomsen et al., 2001; Wilms et al., 2007). We now have verified this assumption by direct measurements of elevated ex situ AOM rates determined at the respective layers of the 20 m-long cores studied here.

4.1 Imprint of past environmental conditions

Microbial abundance and activity (Figs. 5, 6) are linked to paleo-environmental conditions via sediment structure, organic matter quality and geochemical composition. At present, ex situ sulfate reduction rates in both cores are highest in the uppermost layers where sulfate and most likely labile organic material are available for anaerobic respiration. We speculate that the sediments, which are presently found at 5 to 11 mbsf in core JS-A, also exhibited higher sulfate reduction rates during the time of deposition. This assumption is supported by the almost complete depletion of sulfate, the

still elevated TOC content as well as the framboidal structure of pyrites. Even if euhedral pyrite structures show that pyrite formation still occurred after deeper burial of the sediments, the sulfur cycle appears to be primarily controlling microbial and thus biogeochemical dynamics in freshly deposited sediments, i.e. under the environmental conditions prevailing during deposition.

Conclusions about the paleo-microbial activity are, however, hampered by better preservation of microbial and biogeochemical signals in certain lithological layers. For example within mud-dominated sediments of site JS-A (depth interval of 5 to 11 mbsf), this preservation is reflected by high alkalinity and ammonium concentrations which are indicative for remineralization processes. Currently, sulfate reduction rates in these layers are not measureable due to the lack of sulfate and labile organic matter (Fig. 6).

Although sediment type and original organic matter composition has an impact on the microbial community composition in core JS-B, the imprint of the paleo-environment on microbial processes is less pronounced than expected. We did not find a relationship between lithology, microbial abundance, and activity as described e.g. for ash layers in comparison to clay layers in coastal subseafloor sediments (Inagaki et al., 2003). Rather porosity and permeability influence the exchange between different layers due to diffusion and possibly advection barriers. Furthermore, increasing sediment age may have led to decreasing bioavailability and increasing recalcitrance of organic matter. Even though sulfate can still serve as electron acceptor for microbial respiration below a depth of $\sim$3 m, sulfate reduction rates are almost not measurable indicating the lack of a suitable electron donor. Thus, the Eemian mud-rich intervals with elevated TOC contents do not leave an imprint on the current microbial activity. This results in a homogeneous distribution of more or less inactive microbial communities along the depth profile of core JS-B.

4.2 Imprint of present environmental conditions

The imprint of the paleo-environment on microbiology and biogeochemistry is superimposed by environmental conditions that have developed more recently. Our results provide hints that the current hydrogeological situation influences biogeochemistry and microbial activity. Seawater intrusion in deep permeable sands may transport sulfate to formerly sulfate-poor layers (Figs. 2, 3). Deep saltwater encroachments are common in coastal aquifers and are typically explained as re-circulating seawater (Cooper, 1964; Kohaut, 1964; Reilly and Goodman, 1985; Reilly, 1993). At site JS-A, the re-supply of sulfate leads to enhanced sulfate reduction rates in Pleistocene sands below 12 mbsf, reaching almost the same order of magnitude as those in the uppermost meters (Fig. 6). In contrast, no sulfate is replenished in the mud-rich layers from 5 to 11 mbsf where sulfate concentrations are close to zero and thus very low current sulfate reduction rates prevail. Former studies down to 5 m depth indicated that microbial processes in central parts of the Janssand tidal flat are only slightly influenced by pore water flow (Beck et al., 2009). Nevertheless, flow velocities may be fast enough to re-supply sulfate to sites JS-A and JS-B in the central part over long time scales such as several thousands of years.

At site JS-B, the hydrogeological setting and the microbial response are different. The lithological barrier at about 4 mbsf marks the lower boundary of the sulfate reduction zone. The weakly permeable Holocene mud layers inhibit the downward supply of sulfate and dissolved organic material to the Pleistocene sand-dominated layers below. The deep saltwater intrusion described above is also visible in the chloride and sulfate profiles of core JS-B. However, the shapes of the profiles indicate a diffusion-dominated system without microbial sulfate reduction. The current abundance of terminal degraders of organic matter is much lower at site JS-B compared to site JS-A, even though we found similar cell counts in both cores (Fig. 5).

Organic matter degradation is most often syntrophically performed with the help of fermenting microorganisms. Due to the high diversity of pathways and organisms involved in these processes, their analysis is highly challenging. Furthermore, fermentation products do not accumulate in the sediment, which makes their monitoring rather difficult. However, terminal degraders of a metabolically active microbial community are fueled by fermenters and enhanced terminal degradation processes would be detectable by the methods applied here. Our findings indicate that most of the detected microorganisms in core JS-B are presently not active or may even be spores. The latter explanation is supported by viable counts which show that pasteurized incubations exhibit almost the same numbers as non-pasteurized incubations (data not shown). Further, the numbers of endospores increase from about 1% of the total cell counts in Janssand surface sediments to 10% at 5 mbsf indicating an increasing number of bacteria in this resting stage with depth (Fichtel et al., 2008). At site JS-A, pasteurized and non-pasteurized incubations result in similar numbers at 0.5 and 18 mbsf as for site JS-B. However, more viable cells than spores are detected at intermediate sediment depth indicating a more active community.

4.3 The transition between shallow tidal-flat sediments and the deep biosphere

The detection of typical deep-biosphere bacteria such as the *Chloroflexi* in relatively young subsurface tidal-flat sediments was the first evidence for comparable environmental conditions (Wilms et al., 2006a). The astonishing similarities between certain biogeochemical and microbiological features of the upper 5 m of tidal-flat sediments and the upper hundred meters of deep-sea sediments were highlighted by Engelen and Cypionka (2009). They proposed the subsurface

of tidal flats to be a model for the marine deep biosphere. This was further supported by the investigations of Beck et al. (2009). Their analysis of an 80 m transect comprising five cores from the low water line to the top of the Janssand tidal flat suggested stretching of biogeochemical profiles into deeper layers at sites of decreasing microbial activity. The investigated 20 m-long sediment cores fit nicely into this concept, on an intermediate temporal and spatial scale. Sulfate and methane profiles at site JS-A are strikingly similar to several of those described for the deep biosphere (D'Hondt et al., 2004; Parkes et al., 2005; Engelen et al., 2008).

The intermediate range of microbial activities at sites JS-A and JS-B compared to shallower tidal-flat sediments and the deep biosphere is also reflected by the range of sulfate reduction rates. In tidal-flat sediments down to 5 m depth, rates are up to three orders of magnitude higher (Beck et al., 2009) than in the 20 m-long cores. These high rates were obtained at sites influenced by pore water flow and/or fast sedimentation. Without such stimulating processes, rates may be substantially lower as observed previously in central parts of tidal flats. Thus, the ex situ sulfate reduction rates in the 20 m-long core are quite similar to those of the marine deep biosphere (Parkes et al., 2005). The abundance of *Bacteria* and *Archaea* is in the lower range of values typical for the upper 5 m of the tidal-flat subsurface (Wilms et al., 2007) and in the upper end compared to deep-sea sediments (Engelen et al., 2008).

5 Conclusions

Our interdisciplinary approach has shown that the paleo-environment has less impact on current microbial abundance and activity than originally expected. Sediment horizons exhibiting different deposition histories do not lead to a specific microbial response. Instead, the lithological succession influences the present hydrogeological regime in terms of availability of electron donors and acceptors. Thus, the paleo-environmental imprint is still visible but superimposed by modern processes.

Acknowledgements. We thank the team of the Thade-Gerdes GmbH (Norden, Germany) for drilling. R. Bahlo, O. Dellwig, C. Lehners, T. Leipe, C. Lenz, and R. Rosenberg are thanked for their help during the sampling campaign and technical assistance. We further thank the Lower Saxony Water Management, Coastal Defense and Nature Conservation Agency (NLWKN) for providing facilities for core sampling and the University of Münster (Germany) for offering us the possibility to use their Marine Biological Wadden Sea Station. The Wadden Sea National Park Authority of Lower Saxony is thanked for the permission to drill on the Janssand tidal flat. This work was financially supported by Leibniz Institute for Baltic Sea Research, Max Planck Society, and Deutsche Forschungsgemeinschaft (DFG) within the Research Group on "BioGeoChemistry of Tidal Flats".

Edited by: C. P. Slomp

References

Al-Raei, A. M., Bosselmann, K., Böttcher, M. E., Hespenheide, B., and Tauber, F.: Seasonal dynamics of microbial sulfate reduction in temperate intertidal surface sediments: Controls by temperature and organic matter, Ocean Dynam., 59, 351–370, doi:10.1007/s10236-009-0186-5, 2009.

Babu, C. P., Brumsack, H.-J., and Schnetger, B.: Distribution of organic carbon in surface sediments along the eastern Arabian sea: A revisit, Mar. Geol., 162, 91–103, 1999.

Baldock, J. A., Masiello, C. A., Gelinas, Y., and Hedges, J. I.: Cycling and composition of organic matter in terrestrial and marine ecosystems, Mar. Chem., 92, 39–64, 2004.

Beck, M., Dellwig, O., Holstein, J. M., Grunwald, M., Liebezeit, G., Schnetger, B., and Brumsack, H.-J.: Sulphate, dissolved organic carbon, nutrients and terminal metabolic products in deep pore waters of an intertidal flat, Biogeochemistry, 89, 221–238, doi:10.1007/s10533-008-9215-6, 2008a.

Beck, M., Dellwig, O., Liebezeit, G., Schnetger, B., and Brumsack, H.-J.: Spatial and seasonal variations of sulphate, dissolved organic carbon, and nutrients in deep pore waters of intertidal flat sediments, Estuar. Coast. Shelf S., 79, 307–316, doi:10.1016/j.ecss.2008.04.007, 2008b.

Beck, M., Köster, J., Engelen, B., Holstein, J., Gittel, A., Könneke, M., Riedel, T., Wirtz, K., Cypionka, H., Rullkötter, J., and Brumsack, H.-J.: Deep pore water profiles reflect enhanced microbial activity towards tidal flat margins, Ocean Dynam., 59, 371–383, doi:10.1007/s10236-008-0176-z, 2009.

Berg, P., Risgaard-Petersen, N., and Rysgaard, S.: Interpretation of measured concentration profiles in sediment pore water, Limnol. Oceanogr., 43, 1500–1510, 1998.

Billerbeck, M., Werner, U., Polerecky, L., Walpersdorf, E., de Beer, D., and Huettel, M.: Surficial and deep pore water circulation governs spatial and temporal scales of nutrient recycling in intertidal sand flat sediment, Mar. Ecol.-Prog. Ser., 326, 61–76, 2006.

Böttcher, M. E., Hespenheide, B., Llobet-Brossa, E., Beardsley, C., Larsen, O., Schramm, A., Wieland, A., Böttcher, G., Berninger, U. G., and Amann, R.: The biogeochemistry, stable isotope geochemistry, and microbial community structure of a temperate intertidal mudflat: An integrated study, Cont. Shelf Res., 20, 1749–1769, 2000.

Böttcher, M. E., Khim, B. K., Suzuki, A., Gehre, M., Wortmann, U. G., and Brumsack, H.-J.: Microbial sulfate reduction in deep sediments of the Southwest Pacific (ODP Leg 181, Sites 1119–1125): Evidence from stable sulfur isotope fractionation and pore water modeling, Mar. Geol., 205, 249–260, doi:10.1016/s0025-3227(04)00026-x, 2004.

Boudreau, B. P.: Diagenetic models and their implementation – modelling transport and reactions in aquatic sediments, Springer, Heidelberg, Germany, 115–116, 1997.

Bungenstock, F. and Schäfer, A.: The Holocene relative sea-level curve for the tidal basin of the barrier island Langeoog, German Bight, southern North Sea, Global Planet. Change, 66, 34–51, doi:10.1016/j.gloplacha.2008.07.007, 2009.

Cadée, G. C. and Hegeman, J.: Phytoplankton in the Marsdiep at the end of the 20th century; 30 years monitoring biomass, primary production, and *phaeocystis* blooms, J. Sea Res., 48, 97–110, 2002.

Chang, T. S., Flemming, B. W., and Bartholomä, A.: Distinction between sortable silts and aggregated particles in muddy intertidal

sediments of the East Frisian Wadden Sea, southern North Sea, Sed. Geol., 202, 453–463, doi:10.1016/j.sedgeo.2007.03.009, 2007.

Cline, J. D.: Spectrophotometric determination of hydrogen sulfide in natural waters, Limnol. Oceanogr., 14, 454–458, 1969.

Cooper, H. J.: A hypothesis concerning the dynamic balance of fresh water and salt water in a coastal aquifer, U.S. G.S. Water Supply Paper, 1613-C, 1–12, 1964.

D'Andrea, A. F., Aller, R. C., and Lopez, G. R.: Organic matter flux and reactivity on a South Carolina sandflat: The impacts of porewater advection and macrobiological structures, Limnol. Oceanogr., 47, 1056–1070, 2002.

D'Hondt, S., Jørgensen, B. B., Miller, D. J., Batzke, A., Blake, R., Cragg, B. A., Cypionka, H., Dickens, G. R., Ferdelman, T., Hinrichs, K. U., Holm, N. G., Mitterer, R., Spivack, A., Wang, G. Z., Bekins, B., Engelen, B., Ford, K., Gettemy, G., Rutherford, S. D., Sass, H., Skilbeck, C. G., Aiello, I. W., Guerin, G., House, C. H., Inagaki, F., Meister, P., Naehr, T., Niitsuma, S., Parkes, R. J., Schippers, A., Smith, D. C., Teske, A., Wiegel, J., Padilla, C. N., and Acosta, J. L. S.: Distributions of microbial activities in deep subseafloor sediments, Science, 306, 2216–2221, doi:10.1126/science.1101155, 2004.

de Beer, D., Wenzhöfer, F., Ferdelman, T. G., Boehme, S. E., Huettel, M., van Beusekom, J. E. E., Böttcher, M. E., Musat, N., and Dubilier, N.: Transport and mineralization rates in North Sea sandy intertidal sediments, Sylt-Rømø basin, Wadden Sea, Limnol. Oceanogr., 50, 113–127, 2005.

Dellwig, O., Böttcher, M. E., Lipinski, M., and Brumsack, H.-J.: Trace metals in Holocene coastal peats and their relation to pyrite formation (NW Germany), Chem. Geol., 182, 423–442, 2002.

Dellwig, O., Beck, M., Lemke, A., Lunau, M., Kolditz, K., Schnetger, B., and Brumsack, H.-J.: Non-conservative behaviour of molybdenum in coastal waters: Coupling geochemical, biological, and sedimentological processes, Geochim. Cosmochim. Ac., 71, 2745–2761, 2007.

Dittmann, S. (Ed.): The Wadden Sea ecosystem, Springer, Heidelberg, Germany, 1–292, 1999.

Dixit, S. and van Cappellen, P.: Surface chemistry and reactivity of biogenic silica, Geochim. Cosmochim. Ac., 66, 2559–2568, 2002.

Engelen, B. and Cypionka, H.: The subsurface of tidal-flat sediments as a model for the deep biosphere, Ocean Dynam., 59, 385–391, doi:10.1007/s10236-008-0166-1, 2009.

Engelen, B., Ziegelmüller, K., Wolf, L., Köpke, B., Gittel, A., Cypionka, H., Treude, T., Nakagawa, S., Inagaki, F., Lever, M. A., and Steinsbu, B. O.: Fluids from the oceanic crust support microbial activities within the deep biosphere, Geomicrobiol. J., 25, 56–66, doi:10.1080/01490450701829006, 2008.

Fichtel, J., Köster, J., Rullkötter, J., and Sass, H.: High variations in endospore numbers within tidal flat sediments revealed by quantification of dipicolinic acid, Geomicrobiol. J., 25, 371–380, doi:10.1080/01490450802402877, 2008.

Fossing, H. and Jørgensen, B. B.: Measurement of bacterial sulfate reduction in sediments – elevation of a single-step chromium reduction method, Biogeochemistry, 8, 205–222, 1989.

Gallinari, M., Ragueneau, O., Corrin, L., DeMaster, D. J., and Treguer, P.: The importance of water column processes on the dissolution properties of biogenic silica in deep-sea sediments I. Solubility, Geochim. Cosmochim. Ac., 66, 2701–2717, 2002.

Gittel, A., Mussmann, M., Sass, H., Cypionka, H., and Könneke, M.: Identity and abundance of active sulfate-reducing bacteria in deep tidal flat sediments determined by directed cultivation and card-fish analysis, Environ. Microbiol., 10, 2645–2658, doi:10.1111/j.1462-2920.2008.01686.x, 2008.

Grasshoff, K., Kremling, K., and Ehrhardt, M.: Methods of seawater analysis, Wiley-VCH, New York, 159–198, 1999.

Grunwald, M., Dellwig, O., Kohlmeier, C., Kowalski, N., Beck, M., Badewien, T. H., Kotzur, S., Liebezeit, G., and Brumsack, H.-J.: Nutrient dynamics in a back barrier tidal basin of the southern North Sea: Time-series, model simulations, and budget estimates, J. Sea Res., 64, 199–212, 2010.

Huettel, M., Ziebis, W., Forster, S., and Luther, G. W.: Advective transport affecting metal and nutrient distributions and interfacial fluxes in permeable sediments, Geochim. Cosmochim. Ac., 62, 613–631, 1998.

Inagaki, F., Suzuki, M., Takai, K., Oida, H., Sakamoto, T., Aoki, K., Nealson, K. H., and Horikoshi, K.: Microbial communities associated with geological horizons in coastal subseafloor sediments from the Sea of Okhotsk, Appl. Environ. Microb., 69, 7224–7235, doi:10.1128/aem.69.12.7224-7235.2003, 2003.

Ishii, K., Mussmann, M., MacGregor, B. J., and Amann, R.: An improved fluorescence in situ hybridization protocol for the identification of bacteria and archaea in marine sediments, FEMS Microbiol. Ecol., 50, 203–212, 2004.

Jansen, S., Walpersdorf, E., Werner, U., Billerbeck, M., Böttcher, M. E., and de Beer, D.: Functioning of intertidal flats inferred from temporal and spatial dynamics of O_2, H_2S and pH in their surface sediment, Ocean Dynam., 59, 317–332, doi:10.1007/s10236-009-0179-4, 2009.

Kallmeyer, J., Ferdelman, T. G., Weber, A., Fossing, H., and Jørgensen, B. B.: A cold chromium distillation procedure for radiolabeled sulfide applied to sulfate reduction measurements, Limnol. Oceanogr. Meth., 2, 171–180, 2004.

Kohaut, F. A.: The flow of fresh water and salt water in the biscayne aquifer of the Miami area, Florida, U.S. G.S. Water Supply Paper 1613-C, 12–32, 1964.

Köpke, B., Wilms, R., Engelen, B., Cypionka, H., and Sass, H.: Microbial diversity in coastal subsurface sediments: A cultivation approach using various electron acceptors and substrate gradients, Appl. Environ. Microb., 71, 7819–7830, 2005.

Kowalski, N., Dellwig, O., Beck, M., Grunwald, M., Fischer, S., Piepho, M., Riedel, T., Freund, H., Brumsack, H. J., and Böttcher, M. E.: Trace metal dynamics in the water column and pore waters in a temperate tidal system: Response to the fate of algae-derived organic matter, Ocean Dynam., 59, 333–350, doi:10.1007/s10236-009-0192-7, 2009.

Liebezeit, G., Behrends, B., and Kraul, T.: Variability of nutrients and particulate matter in backbarrier tidal flats of the East Frisian Wadden Sea, Senckenberg. Marit., 26, 195–202, 1996.

Llobet-Brossa, E., Rabus, R., Böttcher, M. E., Könneke, M., Finke, N., Schramm, A., Meyer, R. L., Grötzschel, S., Rossello-Mora, R., and Amann, R.: Community structure and activity of sulfate-reducing bacteria in an intertidal surface sediment: A multimethod approach, Aquat. Microb. Ecol., 29, 211–226, 2002.

Loebl, M., Dolch, T., and van Beusekom, J. E. E.: Annual dynamics of pelagic primary production and respiration in a shallow coastal basin, J. Sea Res., 58, 269–282, doi:10.1016/j.seares.2007.06.003, 2007.

Lunau, M., Lemke, A., Walther, K., Martens-Habbena, W., and Simon, M.: An improved method for counting bacteria from sediments and turbid environments by epifluorescence microscopy, Environ. Microbiol., 7, 961–968, doi:10.1111/j.1462-2920.2005.00767.x, 2005.

Lunau, M., Lemke, A., Dellwig, O., and Simon, M.: Physical and biogeochemical controls of microaggregate dynamics in a tidally affected coastal ecosystem, Limnol. Oceanogr., 51, 847–859, 2006.

Lundkvist, M., Gangelhof, U., Lunding, J., and Flindt, M. R.: Production and fate of extracellular polymeric substances produced by benthic diatoms and bacteria: A laboratory study, Estuar. Coast. Shelf S., 75, 337–346, 2007.

Middelburg, J. J., Nieuwenhuize, J., Iversen, N., Hogh, N., De Wilde, H., Helder, W., Seifert, R., and Christof, O.: Methane distribution in European tidal estuaries, Biogeochemistry, 59, 95–119, 2002.

Morono, Y., Terada, T., Masui, N., and Inagaki, F.: Discriminative detection and enumeration of microbial life in marine subsurface sediments, ISME J., 3, 503–511, doi:10.1038/ismej.2009.1, 2009.

Niemann, H., Elvert, M., Hovland, M., Orcutt, B., Judd, A., Suck, I., Gutt, J., Joye, S., Damm, E., Finster, K., and Boetius, A.: Methane emission and consumption at a North Sea gas seep (Tommeliten area), Biogeosciences, 2, 335–351, doi:10.5194/bg-2-335-2005, 2005.

Parkes, R. J., Webster, G., Cragg, B. A., Weightman, A. J., Newberry, C. J., Ferdelman, T. G., Kallmeyer, J., Jørgensen, B. B., Aiello, I. W., and Fry, J. C.: Deep sub-seafloor prokaryotes stimulated at interfaces over geological time, Nature, 436, 390–394, doi:10.1038/nature03796, 2005.

Reilly, T. E.: Analysis of ground-water systems in freshwater-saltwater environments, in: Regional Ground-Water Quality, edited by: Alley, M., Van Nostrand Reinhold, New York, 443–469, 1993.

Reilly, T. E. and Goodman, A. S.: Quantitative analysis of saltwater freshwater relationships in groundwater systems – a historical perspective, J. Hydrol., 80, 125–160, 1985.

Rickard, D. and Morse, J. W.: Acid volatile sulfide (AVS), Mar. Chem., 97, 141–197, doi:10.1016/j.marchem.2005.08.004, 2005.

Rink, B., Seeberger, S., Martens, T., Duerselen, C. D., Simon, M., and Brinkhoff, T.: Effects of phytoplankton bloom in a coastal ecosystem on the composition of bacterial communities, Aquat. Microb. Ecol., 48, 47–60, 2007.

Røy, H., Lee, J. S., Jansen, S., and de Beer, D.: Tide-driven deep pore-water flow in intertidal sand flats, Limnol. Oceanogr.-Meth., 53, 1521–1530, 2008.

Rullkötter, J. (Ed.): Biogeochemistry of tidal flats, Ocean Dynam., 59, 157–427, 2009.

Rusch, A., Forster, S., and Huettel, M.: Bacteria, diatoms and detritus in an intertidal sandflat subject to advective transport across the water-sediment interface, Biogeochemistry, 55, 1–27, 2001.

Sarazin, G., Michard, G., and Prevot, F.: A rapid and accurate spectroscopic method for alkalinity measurements in sea water samples, Water Res., 33, 290–294, 1999.

Schulz, H. D.: Quantification of early diagenesis: Dissolved constituents in marine pore water and signals in the solid phase, in: Marine Geochemistry, 2nd edn., edited by: Schulz, H. D. and Zabel, M., Springer, Heidelberg, 73–124, 2006.

Seeberg-Elverfeldt, J., Schlüter, M., Feseker, T., and Kölling, M.: Rhizon sampling of porewaters near the sediment-water interface of aquatic systems, Limnol. Oceanogr.-Meth., 3, 361–371, 2005.

Sindowski, K.-H.: Geologische Karte von Niedersachsen 1:25 000, Erläuterungsbericht Spiekeroog, Nr. 2212, Hannover, 1972.

Streif, H.: Sedimentary record of Pleistocene and Holocene marine inundations along the North Sea coast of Lower Saxony, Germany, Quatern. Int., 112, 3–28, doi:10.1016/s1040-6182(03)00062-4, 2004.

Streif, H. J.: Das Ostfriesische Küstengebiet, Inseln, Watten und Marschen, Samml. Geol. Führer, 57, 1–376, 1990.

Süß, J., Engelen, B., Cypionka, H., and Sass, H.: Quantitative analysis of bacterial communities from Mediterranean sapropels based on cultivation-dependent methods, FEMS Microbiol. Ecol., 51, 109–121, doi:10.1016/j.femsec.2004.07.010, 2004.

Thomsen, T. R., Finster, K., and Ramsing, N. B.: Biogeochemical and molecular signatures of anaerobic methane oxidation in a marine sediment, Appl. Environ. Microb., 67, 1646–1356, 2001.

Treude, T., Boetius, A., Knittel, K., Wallmann, K., and Jørgensen, B. B.: Anaerobic oxidation of methane above gas hydrates at hydrate ridge, NE Pacific ocean, Mar. Ecol.-Progr. Ser., 264, 1–14, 2003.

van Beusekom, J. E. E., Brockmann, U., Hesse, K.-J., Hickel, W., Poremba, K., and Tillmann, U.: The importance of sediments in the transformation and turnover of nutrients and organic matter in the Wadden Sea and German Bight, Dtsch. Hydrogr. Zeitschr., 51, 245–266, 1999.

Vetriani, C., Jannasch, H. W., MacGregor, B. J., Stahl, D. A., and Reysenbach, A. L.: Population structure and phylogenetic characterization of marine benthic archaea in deep-sea sediments, Appl. Environ. Microb., 65, 4375–4384, 1999.

Wang, Q. W. and Morse, J. W.: Pyrite formation under conditions approximating those in anoxic sediments. 1. Pathway and morphology, Mar. Chem., 52, 99–121, 1996.

Wilkin, R. T., Barnes, H. L., and Brantley, S. L.: The size distribution of framboidal pyrite in modern sediments: An indicator of redox conditions, Geochim. Cosmochim. Ac., 60, 3897–3912, 1996.

Wilms, R., Köpke, B., Sass, H., Chang, T. S., Cypionka, H., and Engelen, B.: Deep biosphere-related bacteria within the subsurface of tidal flat sediments, Environ. Microbiol., 8, 709–719, 2006a.

Wilms, R., Sass, H., Köpke, B., Köster, J.-H., Cypionka, H., and Engelen, B.: Specific bacterial, archaeal, and eukaryotic communities in tidal-flat sediments along a vertical profile of several meters, Appl. Environ. Microb., 72, 2756–2764, 2006b.

Wilms, R., Sass, H., Köpke, B., Cypionka, H., and Engelen, B.: Methane and sulfate profiles within the subsurface of a tidal flat are reflected by the distribution of sulfate-reducing bacteria and methanogenic archaea, FEMS Microbiol. Ecol., 59, 611–621, 2007.